Laser Speckle Photography for Surface Tampering Detection

by

YiChang Shih

B.S. in Electrical Engineering
National Taiwan University, 2009

Submitted to the Department of Electrical Engineering and Computer Science
in partial fulfillment of the requirements for the degree of

Master of Science in Electrical Engineering and Computer Science

at the

MASSACHUSETTS INSTITUTE OF TECHNOLOGY

June 2012

Author .....
Department of Electrical Engineering and Computer Science
May 17, 2012

Certified by .....
Frédo Durand
Professor of Electrical Engineering and Computer Science
Thesis Supervisor

Certified by .....
William T. Freeman
Professor of Electrical Engineering and Computer Science
Thesis Supervisor

Accepted by .....
Leslie A. Kolodziejski
Chairman, Department Committee on Graduate Students

Laser Speckle Photography for Surface Tampering Detection

by

YiChang Shih

Submitted to the Department of Electrical Engineering and Computer Science
on May 17, 2012, in partial fulfillment of the
requirements for the degree of
Master of Science in Electrical Engineering and Computer Science

Abstract

It is often desirable to detect whether a surface has been touched, even when the changes made to that surface are too subtle to see in a pair of before and after images. To address this challenge, we introduce a new imaging technique that combines computational photography and laser speckle imaging. Without requiring controlled laboratory conditions, our method is able to detect surface changes that would be indistinguishable in regular photographs. It is also mobile and does not need to be present at the time of contact with the surface, making it well suited for applications where the surface of interest cannot be constantly monitored.

Our approach takes advantage of the fact that tiny surface deformations cause phase changes in reflected coherent light which alter the speckle pattern visible under laser illumination. We take before and after images of the surface under laser light and can detect subtle contact by correlating the speckle patterns in these images. A key challenge we address is that speckle imaging is very sensitive to the location of the camera, so removing and reintroducing the camera requires high-accuracy viewpoint alignment. To this end, we use a combination of computational rephotography and correlation analysis of the speckle pattern as a function of camera translation. Our technique provides a reliable way of detecting subtle surface contact at a level that was previously only possible under laboratory conditions. With our system, the detection of these subtle surface changes can now be brought into the wild.

Thesis Supervisor: Frédo Durand
Title: Professor of Electrical Engineering and Computer Science

Thesis Supervisor: William T. Freeman
Title: Professor of Electrical Engineering and Computer Science

acknowledgments

Thinking back two years ago, it was in the middle of the summer in 2010, the very first moment in my life stepping into M.I.T. I still clearly remember the excitement from deep of my mind when I first met my advisors Professor Bill Freeman and Professor Frédo Durand. I could not finish my thesis and further my study and knowledge without their supports. The first thing I want to do is to thank both my advisors.

Bill is a very knowledgeable and creative person. He came up with this idea of speckle image, which leads to my master work and brings me a lot of fun. His enthusiasm to the project is the torque guiding me move on in the journey of the project. When I lost my direction and confidence toward the project and disappointed at myself, Frédo has always been very encouraging. Every time after talking with Frédo, I feel full of new ideas and motivation.

Frédo and Bill provide me a lot of freedom to explore my interests and enthusiasm in this field, and be very supportive to all my decisions. I'm really grateful that they spent an hour every week to listening my problems and advise me, even they are extremely busy with their works. More important, I learned how to evaluate an idea and a work from discussion with the two wise and experienced professor.

I want to thank my co-authors, Sam Hasinoff and Abe Davis on completing this thesis. Sam first started the work and pass me tremendous useful experience. His promising results at the beginning inspire me and make me confident on the project. Abe contributes the core part of this work, and we spent many midnights in the lab to improve our system. I would like to thank Dheera Venkatraman and Lijin Chen for the help in system design and implementation.

Graphics lab provide me a super nice and friendly environment for research. We are all proud of our culture, working hard and play hard, enjoying research and life, especially our tea time break and meeting meeting. I would like to thanks Abe, Vlad, Yeuhi, Kevin, Robert, and all the lab mates. Hanging out with them really relieve myself form the pressure of research.

Finally, I want to thank my Dad Thomson Shih and Mom Li-Yin Ko. They always gives me the most warming words from the other side of the Earth, across the ocean across the mountains. With them I have no fear of failure, because I know I always

have a home. And I want to thank Emily Su, you are the lighthouse whenever I'm depressed at life here and get homesick.

Days in M.I.T. and garden state are the most precious experience to me. Not only teaching me the knowledge and provide me an excellent environment for research, M.I.T. help me to know myself again, and to love my research, my friends, and my life.

Contents

1 Introduction **17**

1.1 Related work 18

1.2 Contribution 21

1.3 Overview 22

2 Speckle Image Formation and its Variability **25**

2.1 Review for Speckle Image Formation 25

2.2 Speckle variation with camera movement 26

2.3 Speckle variation with various aperture size 27

2.4 Additional effects due to laser scanner 28

3 Rephotography and Similarity Map Computation **31**

3.1 Vision-based computational rephotography 32

3.2 Speckle-based viewpoint alignment 34

3.3 Similarity Map Computation 36

4 System Implementation **39**

4.1 Static camera setup 39

4.2 Portable system setup 40

5 Results **43**

5.1 Limitations 45

6 Conclusion **53**

A Model of Speckle Image Formation **55**

List of Figures

1-1 We detect surface changes for cases where traditional imaging does not work. Top left: our proposed prototype combines an SLR with a consumer pico laser projector. (a),(b) Images of a wall illuminated by the laser projector. The granular pattern (bottom left), called speckle image, is caused by laser interference scattered by the wall. Between (a) and (b), the wall was touched gently. The speckle similarity map we compute in (c) reveals where the wall was touched. (d)–(f): Without the laser projector, the before and after images (d) and (e) reveal no difference, as shown in the similarity map (f). 19

1-2 Touching the surface causes deformation of its micro-structure, which affects the wavefront of the scattered laser. We show scattered laser wavefront from 2 points x_1, x_2, and camera position x_3. The surface height before touching the surface (a) is different than afterwards (b). This affects the relative position of x_1, x_2, x_3, and changes the resulting speckle image. The position change is at the scale of incident wavelength $\lambda \sim 0.6\,\mu$m, so the speckle image change can be observed. 20

1-3 Speckle images vary over different viewpoints. The bottom row shows the image captured at each viewpoint. 22

2-1 Sensitivity of speckle correlation to camera rotation. as measured using our system under different aperture sizes. The plots show the normalized correlation between the reference image and a second speckle image after different amounts of camera rotation. 28

2-2 Laser speckle captured with larger apertures has more high frequency components but lower contrast. (a) Large aperture, $f/1.8$. (b) Small aperture, $f/16$. The speckle image is taken using Canon 5D MarkII and 100 mm Macro lens. 28

2-3 Geometry for the correlation analysis. Given a camera translation amount δ, aperture size determines the overlapping of sampled speckle fields, which determines the correlation between the first speckle image and the second speckle image warped by d. 29

2-4 Aperture effect on speckle image using a laser scanner. The final exposure is the non-coherent summation of the speckle image at each scanned point. Because of the non-coherent summation, the speckle image with larger aperture has lower contrast. 30

3-1 Sensitivity of speckle correlation to viewpoint change, as measured using our system under different aperture sizes. The plots show the normalized correlation between the reference image and a second speckle image after different amounts of in-plane camera translation. 32

3-2 The plot shows the speckle image contrast with varying depth for several apertures, where the origin is the focused distance. 32

3-3 Visual feedback for computational rephotography. (a) Interface for rephotography of 3D scenes with distinctive features. The green line shows the required forward motion, while the red line shows the required in-plane translation. The blue box is the reference viewport, and the white box is the current viewport. The user adjusts the controller to shrink the lines and match the two viewports. (b) Interface for rephotography of flat scenes using structured light. The inset window shows the difference between the reference pattern and the current pattern. The user adjusts the controller to make this difference smaller. (c) Interface for correlation analysis. The dark blue square shows the location in the current frame that best correlates with the center window of the reference frame (cyan square). The strength of this match increases when we are near the reference viewpoint. The numerical value of the normalized correlation is displayed in the upper right window, which helps the user assess how close they are getting. 35

4-1 System prototypes.(a) Static camera setup. (b) Portable system setup. The portable system consists of a controller with 4 degrees of freedom. The SLR and the laser projector are fixed on the controller. 41

5-1 Our technique can detect tiny surface variations due to light pressure. We put a US quarter dollar coin (weight 5.67 g), shown in (b), onto the box shown in (a), then removed it. The similarity map relating the before and after speckle images (c) reveals the outline of the coin. . . 44

5-2 An experiment showing that our technique can detect surface tampering caused by very light pressure. To measure pressure, we attach a piece of incompressible rubber to a sensitive scale, shown in (b). We press lightly against the wall with the rubber (a), and zero the scale while touching. The readout from the scale (b) shows that the force is 27 gf. Since surface area of the rubber is 1 cm $\times$ 1.3 cm, the pressure is 20.7 gf/cm^2. The similarity map relating speckle images before and after touching the wall (c) shows that the touched area can be identified. 45

5-3 Surface tampering detection on different materials using our system. From top to bottom: a glossy textbook cover with a textured design (we drew an XD on it with the fleshly part of a finger), a stone statue (drew a smile), a brushed aluminum camera (drew a backslash), a black plastic camera charger (drew a cross), and a cement floor (stood on the ground wearing shoes). Speckle is still observable for black objects provided that the exposure time is long enough. Our technique also works well for walls and boxes (Figs. 5-1) From top row downwards: a glossy textbook cover with a textured design (we drew an XD on it with a finger), a stone statue (drew a smile), a brushed aluminum camera (drew a backslash), and a black plastic camera charger (drew a cross). Speckle is still observable for black objects provided that the exposure time is long enough. Our technique also works well for walls and boxes (Figs. 5-1) 47

5-4 By changing the focal length of the lens, our method can handle different spatial resolutions. We use a finger to write symbols of different sizes on the wall shown in (a), and apply our technique using lenses of different focal lengths. (b)(c) shows the similarity map in two cases. In (b) we write "SIGGRAPH ASIA 2011" in a 20 cm $\times$ 15 cm area, and in (c) we draw a heart in a 2 cm $\times$ 1.5 cm area. 48

5-5 Camera viewpoint alignment for flat scenes: (a) door, (b) wall, (c) drawer. For each surface, we first take a reference picture, and then move the system away before gently touching the surface. We then perform the our camera viewpoint alignment scheme on each flat scene to find the viewpoint for the test image. The similarity maps (a)-(c) show that the touched area can be detected by our technique. 48

5-6 Camera viewpoint alignment for a statue of a woman's head (a). We take a reference image, and use a finger to draw a heart on the woman's cheek (in the red rectangle). (b) We calculate the similarity between the reference image and the test images taken without moving the camera, (c) after moving the camera away and using only vision-based rephotography for viewpoint alignment, and (d) using the whole proposed viewpoint alignment method. 49

5-7 Camera viewpoint alignment for two non-planar scenes: (a) a cup (c) a highly textured cylinder. We gently touch the surfaces inside the red rectangle and remove our system from the scene before capturing test images. (b) and (d) show the similarity maps for (a) and (c). Our technique successfully detects the touched regions. 50

5-8 We compare our technique to a forensic fingerprinting technique that uses fluorescent powder. We touch different objects using a finger, and show the tampering detection by our technique at the middle column. Then we brush fingerprint powder on the object to detect the latent fingerprint. Our method struggles with transparent objects, while fingerprint powder often fails on porous surfaces. Bottom 2 rows: In the top row we use a bare finger to touch the surface, while in the bottom row we touch the surface with a gloved finger. Fingerprint powder does not work in the latter case, while our technique works in both cases. 51

A-1 Left: Speckle image formation can be decomposed as 5 main steps: (a) scattering, (b) propagation between surface and camera lens, (c) lens modulation, (d) propagation between lens and sensor, and (e) image formation at sensor. 55

A-2 A speckle image simulated using the 2-D version of speckle image formation equation (Eq. (A.7)), with random surface height and constant incident laser amplitude. The illuminated area is 2 cm by 2 ,cm, and the laser wavelength is 635 nm. The distant between the surface and the camera is 30 cm. 58

List of Tables

3.1 Accuracy of vision-based rephotography, measured by the amount of viewpoint change required by the second stage of our viewpoint alignment . Experiments marked (F) used the feature-based PTAM method, while those marked (S) used our structured light technique. 36

Chapter 1

Introduction

Many scenarios, including law enforcement and security, require detecting whether physical objects have been tampered with, e.g. [1]. Often, the contact is subtle and cannot be detected with the naked eye or by comparing pairs of before and after photographs (e.g. Fig. 1-1(d) and (e)). We propose a new technique to detect surface changes for cases where traditional imaging is insufficient. We make use of the speckle generated by laser illumination and exploit the fact that the precise speckle pattern observed from a given viewpoint depends on the phase of the light wavefront and, therefore, is sensitive to tiny perturbations of the imaged surface (Fig. 1-1(a-c)).

We focus on the situation where surface tampering is subtle, where only the phase, and not the intensity of the light reaching the camera might be altered. To address this problem, we leverage laser speckle imaging (Fig. 1-1). A laser speckle image encodes phase information, because speckle originates from the constructive and destructive interferences of waves reflected at different points of the surface (Fig. 1-2(a)) [2]. Phase differences come from the variation in travel distance, which is affected by tiny changes in the surface geometry. When these waves reflect from a surface they undergo shifts in phase. The amount of shift depends on the distance traveled by each point on the wavefront before it is reflected. Variation in this distance is a function of the reflecting surface geometry, and as such, so is the resulting speckle pattern caused by constructive and destructive interference [2].

If the surface profile is altered by an amount as small as the laser wavelength, the speckle pattern is modified (Fig. 1-2(b)).

Our work is inspired by the use of speckle patterns for the measurement of fluid velocity [3, 4, 5], transparent object movement [6], motion sensing [7], and paper authentication [1]. Most prior work, however, deals with displacement parallel to the image plane and requires rigid and controlled laboratory settings. In contrast, we seek to detect *out-of-plane* modifications to the geometry that arise naturally from surface contact. Moreover, we want the ability to take a reference image of the surface, remove the imaging setup from the scene, and return later to take a new image that will reveal whether the surface was touched or not.

This latter requirement is especially difficult because speckle patterns are extremely sensitive to the position of the camera. As our experiments show, before and after photographs of a surface typically need to be taken from within about half a millimeter for our verification method to succeed. While this tolerance is straightforward to achieve in laboratory settings, using carefully calibrated static cameras, for most practical applications of surface verification, the camera and laser often cannot remain fixed in front of the surface. To achieve high-precision viewpoint alignment, we use a combination of computational rephotography, a technique to guide camera to the desired viewpoint based on relative pose estimation [8], and a new analysis of speckle correlation.

1.1 Related work

Paper authentication The methods closest to our technique are those developed for speckle-based paper authentication [9, 10, 1, 11, 12, 13], in which the roughness pattern for individual pieces of paper, and their corresponding speckle, are used as an identifying signature. In one representative method, the paper must be permanently fixed to an elaborate mechanical plate that fits in a magnetic mount, to ensure accurate viewpoint reproduction [13] (p. 92). Other methods require the object to be moved and placed against a scanner. In contrast, we achieve viewpoint alignment using re-photography and speckle correlation, which alleviates the need for contact or mechanical mounts, and allows us to even handle large, immovable objects, such as a wall, the floor, and a statue.

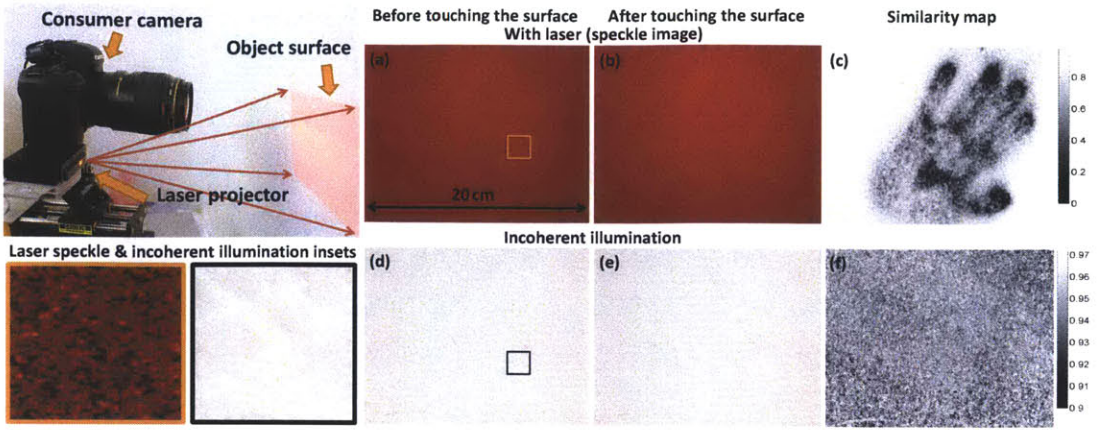

Figure 1-1: We detect surface changes for cases where traditional imaging does not work. Top left: our proposed prototype combines an SLR with a consumer pico laser projector. (a),(b) Images of a wall illuminated by the laser projector. The granular pattern (bottom left), called speckle image, is caused by laser interference scattered by the wall. Between (a) and (b), the wall was touched gently. The speckle similarity map we compute in (c) reveals where the wall was touched. (d)–(f): Without the laser projector, the before and after images (d) and (e) reveal no difference, as shown in the similarity map (f).

Out-of-plane deformation Speckle interferometry can be used to measure out-of-plane deformation (i.e. along the camera optical axis), but current methods require a reference laser under highly calibrated settings, for example, using a beam splitter [14]. We also seek to detect out-of-plane deformations, but with a simpler setup. Our approach can forgo the reference laser because detecting tampering does not require precisely measuring the *amount* of deformation.

Our work differs in two main respects. First, our work does not require a reference laser. Because our task is to identify whether a surface has been touched, rather than accurately measuring the deformation, we do not need to measure the phase difference on the objects. Second, while previous work requires highly accurate calibration for the camera and laser, we develop a system that can work outside of lab settings with a device that can be removed and later returned to perform surface tampering detection.

In-plane motion sensing Speckle patterns can enable the use of traditional computer vision techniques to track objects such as white walls, transparent surfaces, or fluids that would otherwise be featureless. For very small translations parallel to the image plane, the speckle pattern is simply translated

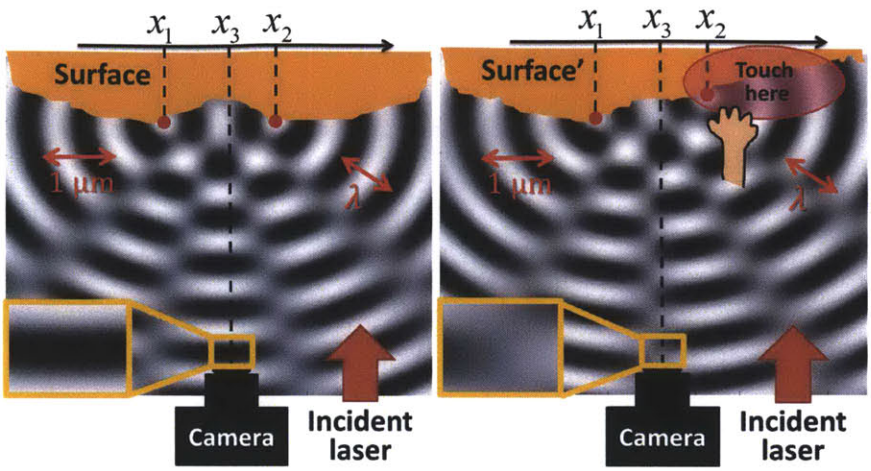

Figure 1-2: Touching the surface causes deformation of its micro-structure, which affects the wavefront of the scattered laser. We show scattered laser wavefront from 2 points x_1, x_2, and camera position x_3. The surface height before touching the surface (a) is different than afterwards (b). This affects the relative position of x_1, x_2, x_3, and changes the resulting speckle image. The position change is at the scale of incident wavelength $\lambda \sim 0.6\,\mu$m, so the speckle image change can be observed.

Shining a laser on these objects, the speckle pattern is a signature of the surface even there are no visible features on the surface. When object displacement is within a certain small range (typically, the size of the laser beam width), the scattered speckle image will follow the motion of the object, allowing small object motions to be measured and tracked with high sensitivity [6]. The applications include in-plane deformation measurement [15], flow visualization [3, 4, 5], and motion sensing [7]. In contrast, our work deals with out-of-plane displacement and camera positioning.

Phase retrieval Since laser speckle depends on the geometry at the scale of the laser wavelength (for us, around 1μm) it may be possible to infer surface geometry from the observed pattern. This inverse problem has been explored, but the phase retrieval this requires is still an open problem [16, 17, 18, 19]. To our knowledge, phase retrieval has only shown potential for simple reflecting surfaces, and as such this work is not applicable to our task.

Speckle modeling We build on models of laser speckles based on Fourier optics [20, 2]. Speckle phenomenon is well studied in the optics community. Goodman [20] explores some of the statistical properties of laser speckle, while [2] examines its formation. Recent work on wave propagation has explored using the Wigner distribution function [21, 22], which combines properties of Fourier optics and the simpler ray-based light field model. Our configuration is simple enough that our analysis can be fully described using Fourier optics.

Computational rephotography In order to capture the new speckle image from the same viewpoint as the reference, we build on computational rephotography methods [8, 23], using the publicly-available PTAM library to perform relative camera pose estimation [24]. While rephotography methods are successful at achieving a coarse viewpoint match, reliable comparison of two speckle patterns requires precision in viewpoint that cannot be achieved with current vision-based techniques. To address this limitation, we exploit the laser projector to refine the viewpoint using correlation analysis of the speckle images.

Forensics One potential application of our technique is in crime scene to determine tampered objects. Skin contact usually leaves traces of body fluids that can be detected using fluorescent fingerprint powder and UV light, or other chemical methods. These approaches are limited to bare-skin contact and non-porous surfaces.

1.2 Contribution

Our thesis makes the following contributions:

- We present a speckle imaging system that is portable and can be moved in practice. After taking a *reference* image, the user can remove all equipment from the scene, and return later to take a *test* image. We display a visualization allowing the user to decide whether the surface has been tampered with.
- We present a new method achieving viewpoint alignment within 0.5 mm using a combination of computational rephotography and speckle correlation analysis.

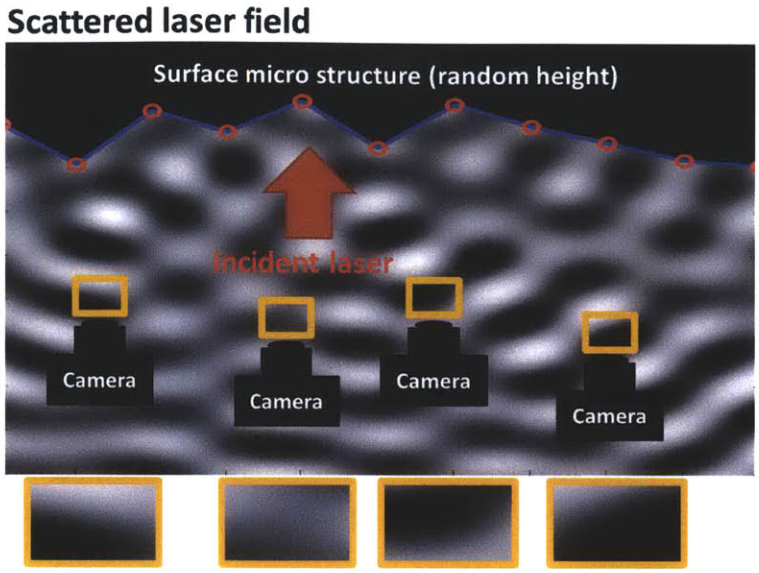

Figure 1-3: Speckle images vary over different viewpoints. The bottom row shows the image captured at each viewpoint.

1.3 Overview

Our main imaging setup relies on a standard digital SLR and a consumer micro laser projector (Fig. 1-1). We currently use a second camera for rephotography, mounted rigidly to the imaging system (Fig. 5-7). In principle, a single camera could be used for both rephotography and speckle imaging, but we found that using a second camera helped us sidestep low-level software issues. The two cameras and projector are rigidly mounted on actuators to enable precise displacements during the final phase of viewpoint alignment. In our prototype, the setup is placed on a cart for easier portability.

The user first takes a reference speckle image where the surface is illuminated by the laser projector. The user then leaves with the camera-projector setup. The surface might then be tampered with or not, and the goal is to determine whether tampering has occurred. Later, the user comes back and needs to take a new speckle image from the same location to detect if the surface was touched. We first use vision-based rephotography [8, 23] to guide the camera to a roughly accurate viewpoint within 3 mm. For flat surfaces where vision-based pose estimation is degenerate, we use structured light and the visual alignment of a checkerboard pattern instead. In

both cases, we then perform a novel correlation analysis between the current laser speckle image and the reference. The correlation depends on the distance between the viewpoints and lets us provide feedback to the user to help them move even closer to the desired viewpoint.

We display the results of tampering detection by running normalized cross correlation between the reference and the final test speckle image (Fig. 1-1c).

Chapter 2

Speckle Image Formation and its Variability

2.1 Review for Speckle Image Formation

We review the equations of speckle image formation [20, 2] in order to analyze how the speckle pattern varies with camera translation and aperture choice. Detailed derivations are provided in the appendix. The one dimensional speckle image $I(y)$ caused by a surface with surface height $h(x)$ is

$$I(y) = \left\| f\left(-\frac{z_1}{z_2}y\right) \otimes \tilde{g}\left(\frac{y}{z_2\lambda}\right) \right\|^2 , \tag{2.1}$$

where

$$f(x) = \frac{A_0}{z_1} e^{jk\left(h(x)+\frac{x^2}{2z_1}\right)} \tag{2.2}$$

is the input function, x and y are the coordinates on the object and image plane respectively, A_0 is the incident wave amplitude, z_1 and z_2 are distances from the lens to the object and to the sensor respectively, and λ is the incident wavelength. We use $\otimes$ to denote convolution and $\tilde{g}(\omega) = \mathbb{F}\{P\}$ is the Fourier transform of the aperture function $P(u)$.

Eq. (2.1) decomposes speckle formation into three steps: (1) the input $\frac{A_0}{z_1}e^{jkh(x)}$ is modulated by a quadratic phase $e^{jk\frac{x^2}{2z_1}}$ and an attenuation $\frac{1}{z}$; (2) it passes through

a low-pass filter $\tilde{g}(\omega)$ determined by the aperture; (3) the speckle image intensity is the squared amplitude of the field. The low-pass filter (2) comes from the fact that the field at the lens is the Fourier transform of the surface field and it gets clipped by the aperture. This model demonstrates locality: the modification of the surface $h(x)$ at a point x only affects the image near $-\frac{z_2}{z_1}x$ because a finite aperture causes $\tilde{g}$ to fall off rapidly, which is important for our application. This is an advantage of using a lens over without a lens when sampling the speckle field.

The form of Eq. (2.1) suggests that the inverse problem, namely, recovering the detailed surface height from speckle images, would be extremely hard. To compute this inverse, we would need to solve phase retrieval and perform deconvolution, both of which are ill-posed problems.

2.2 Speckle variation with camera movement

Using Eq. (2.1), we can derive the speckle image for most situations. Here we address some issues relevant to our work. Fig. 3-1 illustrates speckle variation due to the translation of camera view point measured by our prototype camera.

Camera in-plane translation When the camera moves by δ in the lens plane, we simply need to replace the aperture in Eq. (2.1) by $P(u-\delta)$. As the camera moves, the aperture selects different windows over the field. If the translation is larger than the aperture, the windows don't overlap (Fig. 1-3). Furthermore, these windows are generally uncorrelated because, in practical applications, the surface height $h(x)$ is randomly distributed, and the corresponding speckle images are also uncorrelated. For our surface tampering detection, we need the speckle from untouched regions to be highly correlated in the before/after pair, and the captured windows of the field must be very close.

To understand the effect of camera translation, we analyze the case where the camera remains static and the surface is translated by $-\delta$. The input f in Eq. (2.1) is translated, but the quadratic phase term $\frac{x^2}{2z_1}$ in $f(x)$ in Eq. (2.1) makes the system not shift-invariant and the speckle is altered.

In the optics community, Okamoto and Asakura [25] have proposed a wavefront

modulation known as translational speckle to make the system shift-invariant, so that under camera translation the speckle image undergoes translation only. This approach involves combining an incident laser with a convex lens whose negative quadratic phase wavefront matches the focusing distance precisely. However, translational speckle is not suitable for our application because the lens need to be twice as big as the imaged area, and cannot work for large area on the surface.

Depth translation With the camera in focus, Eq. (2.1) shows that changing the lens-object distance z_1 causes speckle magnification and alteration. Fortunately, this alteration is not as strong as that associated with in-plane translation. The quadratic phase term $e^{jk\frac{z_1 y^2}{2z_2^2}}$ is less affected by depth z_1 than by in-plane translation y. Hence, the required precision for viewpoint alignment is looser along depth and can be achieved with vision-based rephotography alone.

Camera rotation For a radially-symmetric lens, in-plane camera rotation causes only rotation of the speckle image. Out-of-plane rotations of a small angle mostly causes a 2D translation of the speckle image if the lens is not wide angle [26, 2] (Fig.2-1), i.e. for small angles the homography can be approximated by a 2D translation. This can be formalized by analyzing the speckle image formation equations above. When the camera rotates about its center of projection, the field captured by the lens is almost unchanged.

2.3 Speckle variation with various aperture size

Speckle images taken at different apertures can be derived by evaluating Eq. (2.1) with appropriate $P(u)$. From Eq. (2.1), the aperture is equivalent to a low-pass filter, and larger apertures correspond to filters with larger bandwidth. This is equivalent to the well-known reduced diffraction with large apertures. As shown in Fig. 2-2, images with smaller apertures have lower frequency speckle.

Aperture size also plays a role in speckle images decorrelation with respect to camera view point translation. As shown in Fig. 2-3, the aperture size determines the overlap area of the sampled speckle field given a fixed amount of camera view point

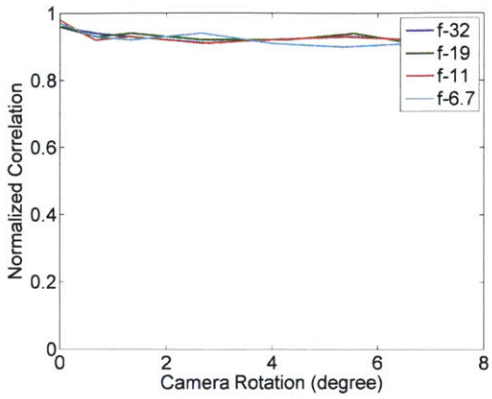

Figure 2-1: Sensitivity of speckle correlation to camera rotation. as measured using our system under different aperture sizes. The plots show the normalized correlation between the reference image and a second speckle image after different amounts of camera rotation.

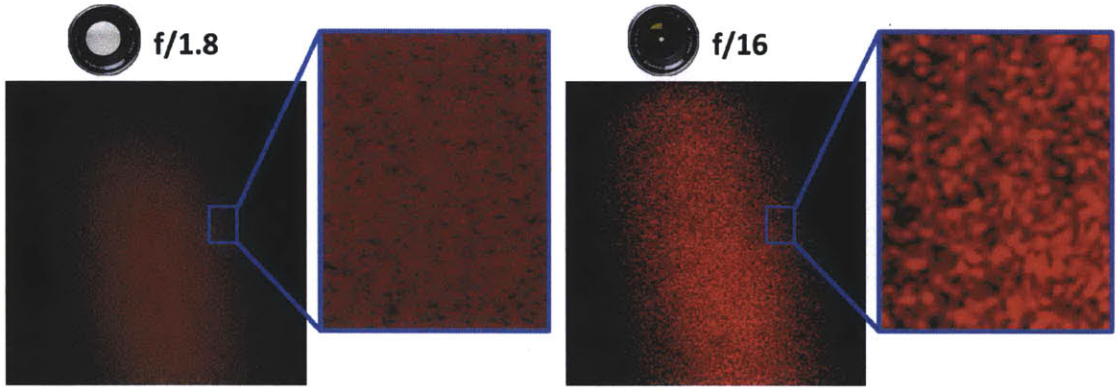

(a) (b)

Figure 2-2: Laser speckle captured with larger apertures has more high frequency components but lower contrast. (a) Large aperture, $f/1.8$. (b) Small aperture, $f/16$. The speckle image is taken using Canon 5D MarkII and 100 mm Macro lens.

translation.

2.4 Additional effects due to laser scanner

Our speckle image formation modeling is based on a point source laser. In this thesis, we want to detect the surface area about 30 cm by 30 cm, so we use a laser scanner

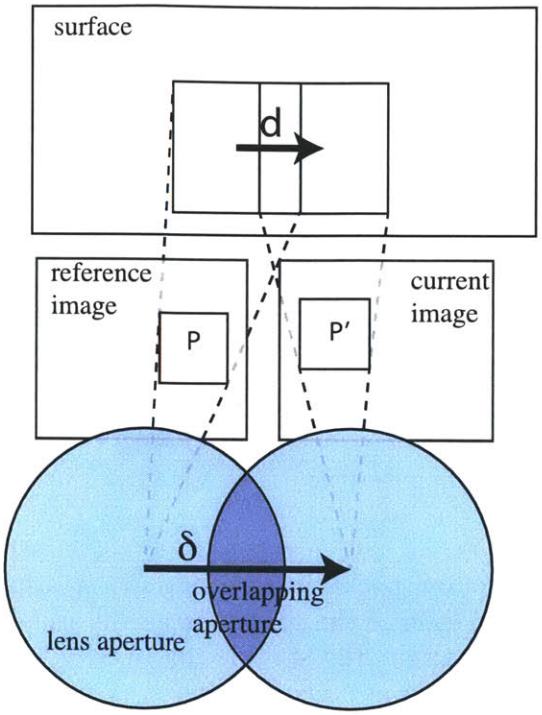

Figure 2-3: Geometry for the correlation analysis. Given a camera translation amount δ, aperture size determines the overlapping of sampled speckle fields, which determines the correlation between the first speckle image and the second speckle image warped by d.

(laser projector) instead of a point source laser. When using a laser projector, speckle contrast reduces when aperture size increases, as shown in Fig. 2-4.

At any instance, the laser projector scan one point on the surface, and generates a corresponding speckle image on the sensor. Because of the finite point spread function (PSF), each point on the image is the mostly-incoherent summation of N speckle image, where N is in proportion to aperture size. That is, the laser illumination at one instant in time interferes coherently, but the N images are not coherent enough over time and their intensity, not their field, get summed. Speckle contrast becomes lower when more independent speckle images are added together.

Given the same translational displacement between reference and target viewpoints, correlation between the two images is higher for larger apertures, because the field captured by the apertures have more overlap, as explained in the previous section.

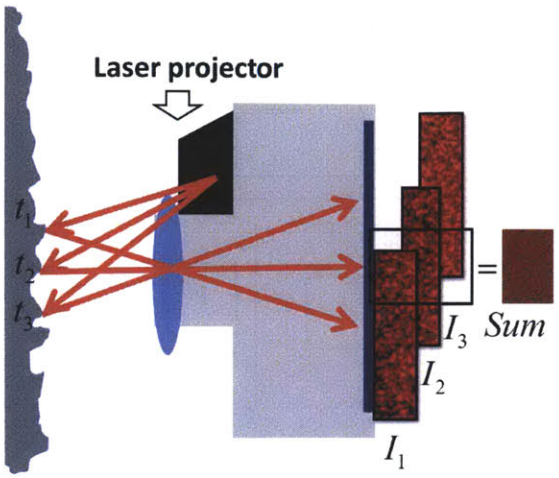

Figure 2-4: Aperture effect on speckle image using a laser scanner. The final exposure is the non-coherent summation of the speckle image at each scanned point. Because of the non-coherent summation, the speckle image with larger aperture has lower contrast.

However, increasing aperture size reduces speckle contrast, which leads to a trade-off, since contrast is needed to identify tampering. In our work, we use a 100 mm lens and found that apertures between $f/6.7$ and $f/16$ work well.

Chapter 3

Rephotography and Similarity Map Computation

One of our main challenges is to achieve the desired camera viewpoint to take the test image. As shown in Fig. 3-1, the reference and test images become decorrelated when the viewpoints differ by more than 1 mm, which sets tight accuracy goals for camera alignment. Typically, to generate two comparable speckle images for surface tampering detection, the distance between the viewpoints must be less than 0.5 mm. To our knowledge, no computational rephotography [8] technique can achieve such accuracy. We propose a two-stage method: first, we adopt vision-based rephotography to get within a few mm, and second, we introduce a speckle-based correlation analysis for finer accuracy.

For the surface tampering detection, the viewpoints between reference and target speckle image must be very close. By comparing speckle contrast between reference and target image can guide camera depth accurate to within 1 mm, which is good enough for surface tampering detection, as shown in Fig. 3-2. Now only camera rotation and translation in lens plane need to be considered. To guide our camera back to the original position as close as 0.5 mm., we propose a 2-stage viewpoint localization. The first stage we use PTAM technique, which exploits the features under incoherent light. Depends on scene features, PTAM usually can guide the camera to within 10 cms away from reference viewpoint. In the second stage, we utilize the speckle image for localization, which can guide our camera to within $10^{-}1$mm.

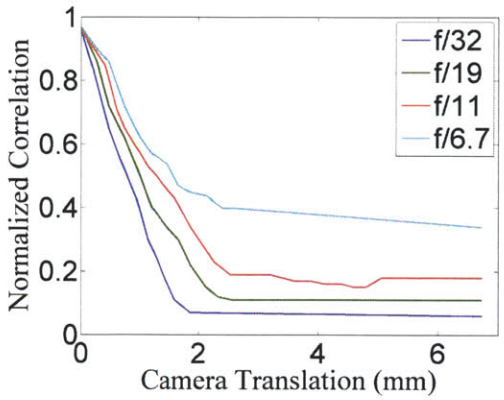

Figure 3-1: Sensitivity of speckle correlation to viewpoint change, as measured using our system under different aperture sizes. The plots show the normalized correlation between the reference image and a second speckle image after different amounts of in-plane camera translation.

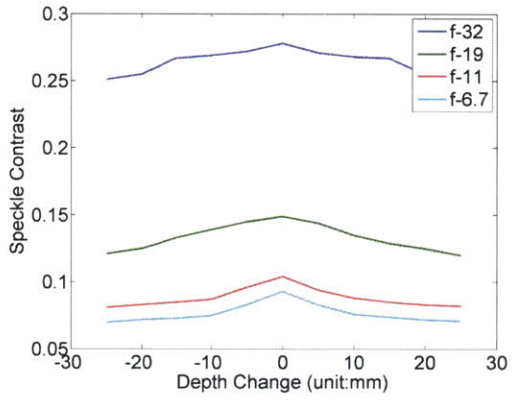

Figure 3-2: The plot shows the speckle image contrast with varying depth for several apertures, where the origin is the focused distance.

3.1 Vision-based computational rephotography

For the first stage, we use two rephotography techniques for different types of scenes. For general 3D scenes with distinctive image features, we use a solution similar to Bae et al. [8] and rely on these features to estimate the relative camera pose. For flat scenes, where pose estimation is degenerate, we project structured light onto the surface and rely on the user to visually match the observed projected pattern. We found that both of these techniques have similar accuracy, and can typically guide

the camera back to the reference viewpoint to within a translation of 3 mm and a rotation of 0.5 degrees (Table 3.1).

Image-based feature matching and pose estimation Our feature-based approach builds on previous methods for feature detection and camera pose estimation, namely the parallel tracking and mapping (PTAM) library [24]. PTAM builds a 3D map where feature points are characterized by 2D image patches. It uses a combination of tracking, RANSAC and bundle adjustment to continuously refine the map and compute the pose of the current camera .

Prior to taking the reference image, we use PTAM to build up a sparse 3D map of feature points from a set of uncalibrated wide-angle photos surrounding the object. We then record the camera pose, turn on the laser projector, and take the reference speckle image.

When we return to take the test image, the current camera pose is estimated by PTAM using the earlier map. We display a 3D visualization of the current displacement from the reference pose, and manually adjust the camera viewpoint until the pose returns to the reference viewpoint.(Fig. 3-3a). Similar to Bae et al. [8], we display the required translation along the optical axis (the green line in Fig. 3-3a), and the required in-plane translation (the red vector). In order to correctly orient the camera, we overlay a 3D visualization of the original viewport, and the user has to align it with the current viewport in white. This method works well when the scene has enough features and depth range. It typically takes us a few minutes to reach the viewpoint with 3 mm accuracy.

Structured light for flat scenes Flat scenes, such as walls, present a special challenge for viewpoint alignment since small camera rotations and translations are ambiguous for flat surfaces. This ambiguity limits viewpoint alignment, which is why we propose to project structured light onto the surface to help resolve the ambiguity. In practice, we use the laser projector to project a checkerboard pattern onto the scene and capture an image of this pattern from the reference viewpoint At test time, matching the appearance of the projected checkerboard lets us resolve the translation-rotation ambiguity. Because the camera and the projector are not co-located, the

resulting parallax deforms the observed pattern when the system is moved. However, when the system translates in a direction parallel to the flat surface, the observed pattern is invariant. In order to resolve these remaining two degrees of freedom, we use a single 2D feature on the surface, e.g. a door knob. We use the same projector for speckle imaging so only one is needed for the whole system. Note that the geometric relation between the camera and the projector is fixed, so there is no transform between taking the reference pattern and taking the test pattern. The alignment is currently based on visual matching and manual displacement, but it could be automated in future work. We display a difference image between the reference view of the checkerboard and the current view to assist the user (Fig. 3-3b).

Camera rotation Speckle decorrelation is less sensitive to camera rotation. Hence, in the scene that has enough features, PTAM can give us good precision in camera rotation. For the scene with a big flat surface with few features, such as door or wall, we use our system to project a chessboard image on the surface and take the reference chessboard image before taking the reference image for surface tampering detection. When we take the target image, we project the same chessboard image, rotate the camera and take target chessboard images. By comparing these target chessboard image with reference chessboard image, we can find out the desired camera rotation.

3.2 Speckle-based viewpoint alignment

In the second stage of viewpoint alignment, we focus on refining the in-plane camera translation by analyzing the correlation between the current speckle image and the reference one. This provides users with feedback as to whether they are getting closer or farther from the reference viewpoint. As described in section 2.2, speckle correlation is less sensitive to depth change, so the first stage of viewpoint alignment provides sufficient accuracy for this degree of freedom.

Within the uncertainty range given by the first stage, we sample along the camera plane (perpendicular to the optical axis). For each sampled image we display its normalized cross correlation (NCC) with the reference speckle image as feedback to the user. The NCC is computed as below,

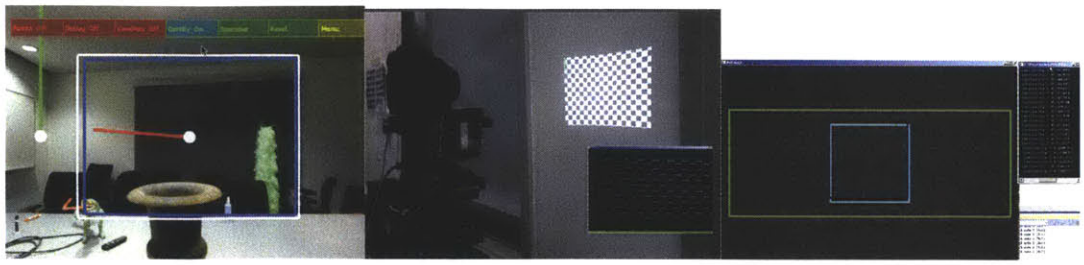

(a) (b) (c)

Figure 3-3: Visual feedback for computational rephotography. (a) Interface for rephotography of 3D scenes with distinctive features. The green line shows the required forward motion, while the red line shows the required in-plane translation. The blue box is the reference viewport, and the white box is the current viewport. The user adjusts the controller to shrink the lines and match the two viewports. (b) Interface for rephotography of flat scenes using structured light. The inset window shows the difference between the reference pattern and the current pattern. The user adjusts the controller to make this difference smaller. (c) Interface for correlation analysis. The dark blue square shows the location in the current frame that best correlates with the center window of the reference frame (cyan square). The strength of this match increases when we are near the reference viewpoint. The numerical value of the normalized correlation is displayed in the upper right window, which helps the user assess how close they are getting.

$$NCC(f_1, f_2) = \frac{\Sigma_i[f_1(i) - \overline{f_1}][f_2(i) - \overline{f_2}]}{\{\Sigma_i[f_1(i) - \overline{f_1}]^2 \Sigma_i[f_2(i) - \overline{f_2}]^2\}^{0.5}} \tag{3.1}$$

As shown in Fig. 3-1, NCC reaches its maximum when the viewpoints are the same. Hence, by maximizing the NCC, we can determine the desired position. In our work we sample every 0.5 mm in the range [-5 mm, 5 mm]. When computing the NCC, we first crop a patch in the sampled image and then search for the patch in the reference image that results in the maximum NCC with our sampled patch. The NCC value is displayed as feedback to the user. This helps the user resolve any misalignment between two speckle images due to the small rotation uncertainty given by the first stage.

After determining the camera translation, the user corrects the camera rotation by matching 2D features from the current frame with the reference frame.

In summary, to determine the viewpoint for rephotography, vision-based camera

experiment		translation, horizontal (mm)	translation, vertical (mm)	rotation (arcmin)
Statue	(F)	2.5	0.2	23
Cup	(F)	2.1	0.3	20
Cylinder	(F)	1.3	0.5	17
Door	(S)	1.2	0.1	12
Wall	(S)	1.1	0.2	13
Drawer	(S)	1.7	0.1	18

Table 3.1: Accuracy of vision-based rephotography, measured by the amount of viewpoint change required by the second stage of our viewpoint alignment . Experiments marked (F) used the feature-based PTAM method, while those marked (S) used our structured light technique.

pose estimation is first used to roughly localize the camera, and then correlation analysis and dense sampling are used to refine the viewpoint.

3.3 Similarity Map Computation

Once the correct viewpoint has been reached, we take the test speckle image. We carefully align this image to our reference image before analyzing their differences.

To match the speckle images we randomly sample image patches, match those patches, and fit a warp to the resulting patch correspondences. As Eq. (2.1) shows, touching the surface only affects the speckle image near the touched area, so local comparisons are sufficient for matching. First, we sample several hundred patches from the reference image, then for each patch we use normalized cross correlation to find the corresponding best-matching patch in the test image. Given these correspondences, we use RANSAC to recover a 3×3 homography relating the two speckle images, while ignoring potential outliers due to tampering.

We then compute the similarity map S relating the target image I_{tar} and the warped reference image $I_{\text{ref,w}}$,

$$S(i,j) = NCC(W(i,j)I_{\text{tar}}, W(i,j)I_{\text{ref,w}}) \ , \tag{3.2}$$

where NCC computes the normalized cross correlation, and $W(i,j)$ is a windowing function centered at (i,j). For our results we used a window size of 21×21 pixels.

The smaller window provides higher spatial resolution while being more vulnerable to noise.

While computing NCC costs more computation than simply displaying the difference between two speckle images, NCC provides the following advantages over displaying the difference. First, NCC is more robust to image warping error. Second, NCC is more robust to the ambient light change between before/after speckle images. Also, NCC scales the similarity map between zeros and one, which is convenient for visualization.

Chapter 4

System Implementation

We design two setups using laser speckle photography for surface tampering detection. In the static setup the camera is fixed to the surface, and so no computational rephotography is needed. The purpose of this setup is to show laser speckles are sensitive to subtle surface change. In the second setup the system is portable, and so the camera can be removed between the two speckle images. We show our computational rephotography on our portable system setup.

4.1 Static camera setup

The static setup is shown in Fig. 4-1a. The camera is mounted on a copy stand, and we use the MicroVision ShowWX+ as our projector. We use Canon EOS 5D Mark II and Canon Ultrasonic 100 mm Macro Lens. Under normal indoor lighting condition, we choose aperture to be f/32, ISO 100, and exposure time 1 second. We calibrate the camera and the projector once before starting to use the system. The system takes a first reference speckle image, and then the user can tamper the surface. Then the system takes the second speckle image, computing the similarity map, and then project the map to the surface. The projected image informs the user the tampered region on the surface. The camera is controlled using Canon SDK 2.10.

4.2 Portable system setup

Our portable prototype is shown in Fig. 4-1b. We use the Microvision PicoP® [27] as our laser projector and the Canon EOS 5D Mark II® for capturing the speckle image. For camera registration, we use a motorized labjack to adjust the vertical position of the camera, two motorized translation stages to adjust the depth and horizontal position, and a motorized rotation stage to adjust camera rotation. The precision of the labjack and translation stage is 0.01 mm, and the rotation stage has a measurement precision of 1 degree but a higher precision for actuation. We put the whole system on a cart for mobility.

While we could use the same camera for speckle imaging and for rephotography, we have found that using a second camera rigidly-linked to the first one is easier. It allows us to use a wider-angle lens for rephotography, thereby including more features for pose estimation. From a practical standpoint, it also made it possible to run code for rephotography and speckle imaging on different computers, avoiding the problematic sharing of a single camera interface between two threads.

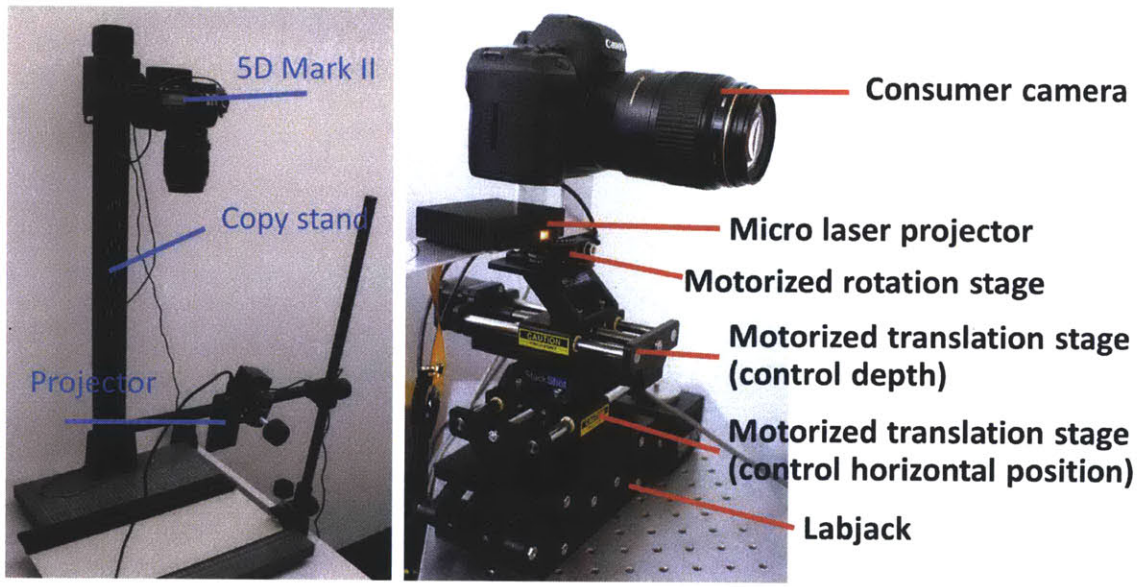

(a) Static camera setup

(b) Portable system setup

Figure 4-1: System prototypes.(a) Static camera setup. (b) Portable system setup. The portable system consists of a controller with 4 degrees of freedom. The SLR and the laser projector are fixed on the controller.

Chapter 5

Results

We performed a number of tests to evaluate surface tampering detection and viewpoint alignment using our system.

First, we tested the sensitivity of our similarity map (Eq. (3.2)) to demonstrate its ability to detect subtle surface changes resulting from small forces. To study this sensitivity independent of issues with viewpoint alignment, we kept the camera fixed on a tripod while photographing the reference (before surface deformation) and test (after) images. In the experiment of Fig. 5-1, we placed a quarter (5.67 g) on a heavy cardboard box. The similarity map of the test to reference images clearly reveals the effect of the quarter's weight on the box. Only the boundary of the quarter is visible because the coin is thicker at the periphery and does not touch the surface in the center. To avoid extra forces on the box we taped the coin to a string, lowered it slowly onto the box, and removed it by lifting the string.

The experiment of Fig. 5-2 reveals the effect of touching a sheet rock wall with a rubber square using the lightest force we could measure with a hand-held pressure scale apparatus. The mark from the 20.7 gf/cm^2 pressure (gf = gram-force) is clearly visible in the normalized correlation similarity map.

Fig. 5-3 shows the results of our system detecting finger-pressure marks on surfaces of different shapes, colors, and materials. The results show speckle works on various kinds of materials.

Changing the focal length of the lens also allows the technique to work at different spatial scales easily, as shown in Fig. 5-4.

(a) box (b) quarter dollar (c) similarity map

Figure 5-1: Our technique can detect tiny surface variations due to light pressure. We put a US quarter dollar coin (weight 5.67 g), shown in (b), onto the box shown in (a), then removed it. The similarity map relating the before and after speckle images (c) reveals the outline of the coin.

The remaining figures demonstrate the reliability of our viewpoint alignment schemes for surface tampering detection. Fig. 5-5 shows the effectiveness of the structured light method for viewpoint alignment with flat scenes. The surface tampering detection reveals light finger touches to a wooden door, a wall, and a steel filing cabinet.

Figs. 5-6 and 5-7 show the results of using our vision-based rephotography to reveal light finger marks on 3D surfaces. Surprisingly, we found that pushing harder makes little difference. Essentially, once the surface modification is large enough compared to the wavelength of the laser, additional modifications have limited impact.

In all these viewpoint alignment experiments, the two-stage camera alignment procedure was used, with the first stage of the alignment procedure being specialized to flat or 3D scenes, appropriately. The average time for two-stage camera alignment in both cases is around 5 minutes. Typically, both of the first-stage rephotography options, feature-based PTAM and our structured light technique, allow us to bring the camera back to within 3 mm, as shown in Table 3.1.

Comparison with UV light and fingerprint powder As a potential application in forensic technique, we compare our work against a leading forensic technique for fingerprinting that uses fluorescent powder. When a human touches an object, some fluids from the finger are transferred to the object's surface. Later, the surface can be brushed with a fluorescent powder that is adhesive to fluid. A Shining a UV light on the brushed surface will then reveal the pattern of fluid left by the finger. This

Figure 5-2: An experiment showing that our technique can detect surface tampering caused by very light pressure. To measure pressure, we attach a piece of incompressible rubber to a sensitive scale, shown in (b). We press lightly against the wall with the rubber (a), and zero the scale while touching. The readout from the scale (b) shows that the force is 27 gf. Since surface area of the rubber is 1 cm $\times$ 1.3 cm, the pressure is 20.7 gf/cm^2. The similarity map relating speckle images before and after touching the wall (c) shows that the touched area can be identified.

method is low cost and often used in forensic investigation.

As shown in Fig. 5-8, our method and the fingerprint powder technique have different limitations. Our approach does not work on transparent objects because there is no reflected laser light, whereas fingerprint powder works well. Porous surfaces, on the other hand, present the opposite scenario because fluids do not stick to them well, and, moreover, the powder tends to stick even in the absence of fluid. In contrast, our method works well for such surfaces. Fig. 5-8 also shows that the fingerprint powder fails to reveal the touch of a gloved hand, while the speckle change is clearly visible.

Fingerprint powder does not require a reference image and is often able to recover the detailed groove pattern of a fingerprint. However, unlike our technique which does not require any contact with the scene, fingerprint powder is potentially destructive to the surface being examined.

5.1 Limitations

Unfortunately, very accurate camera registration is an unavoidable requirement. In Section 2.1, we showed that speckle image is the power spectral density of the field sampled by the aperture at lens plane, and the field on the lens plane is the Fourier transform of the surface phase function multiplied by a quadratic phase function. For most materials in daily life, the surface phase function is a random function, and the field on the lens plane is a random function. If the camera is not registered, then both

the sampled fields and the speckle images are uncorrelated, and surface certification fails.

We showed that our system works well for a variety of common materials. However, we have found that our system struggles with the following three types of materials. (1) Volumetric materials, such as carpets, sweaters, and scarves. For these materials, the surface is not well defined, and our camera cannot observe speckle. (2) Reflective and transparent materials, such as mirrors, shiny metals or glass. For these kinds of materials, the speckle cannot not be observed. (3) Materials that absorb light at the bandwidth of our laser, such as cyan material for a red laser, or black materials for all bandwidths. For these materials, speckle can be observed only with long enough exposure and under very low ambient light condition. In general, diffuse and moderately-glossy surfaces that are not too dark work best.

Figure 5-3: Surface tampering detection on different materials using our system. From top to bottom: a glossy textbook cover with a textured design (we drew an XD on it with the fleshly part of a finger), a stone statue (drew a smile), a brushed aluminum camera (drew a backslash), a black plastic camera charger (drew a cross), and a cement floor (stood on the ground wearing shoes). Speckle is still observable for black objects provided that the exposure time is long enough. Our technique also works well for walls and boxes (Figs. 5-1) From top row downwards: a glossy textbook cover with a textured design (we drew an XD on it with a finger), a stone statue (drew a smile), a brushed aluminum camera (drew a backslash), and a black plastic camera charger (drew a cross). Speckle is still observable for black objects provided that the exposure time is long enough. Our technique also works well for walls and boxes (Figs. 5-1)

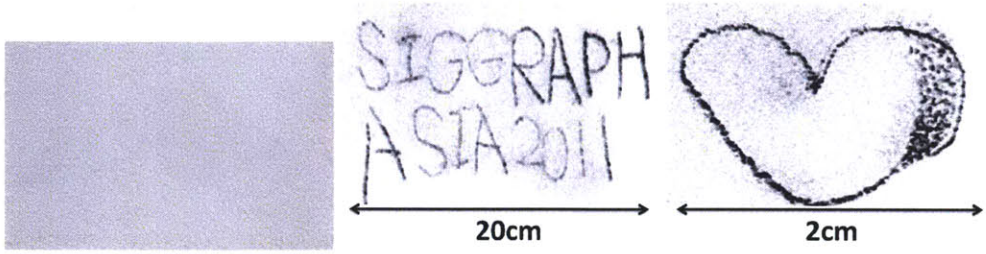

(a) wall (b) $f = 28\,\text{mm}$ (c) $f = 100\,\text{mm}$

Figure 5-4: By changing the focal length of the lens, our method can handle different spatial resolutions. We use a finger to write symbols of different sizes on the wall shown in (a), and apply our technique using lenses of different focal lengths. (b)(c) shows the similarity map in two cases. In (b) we write "SIGGRAPH ASIA 2011" in a $20\,\text{cm} \times 15\,\text{cm}$ area, and in (c) we draw a heart in a $2\,\text{cm} \times 1.5\,\text{cm}$ area.

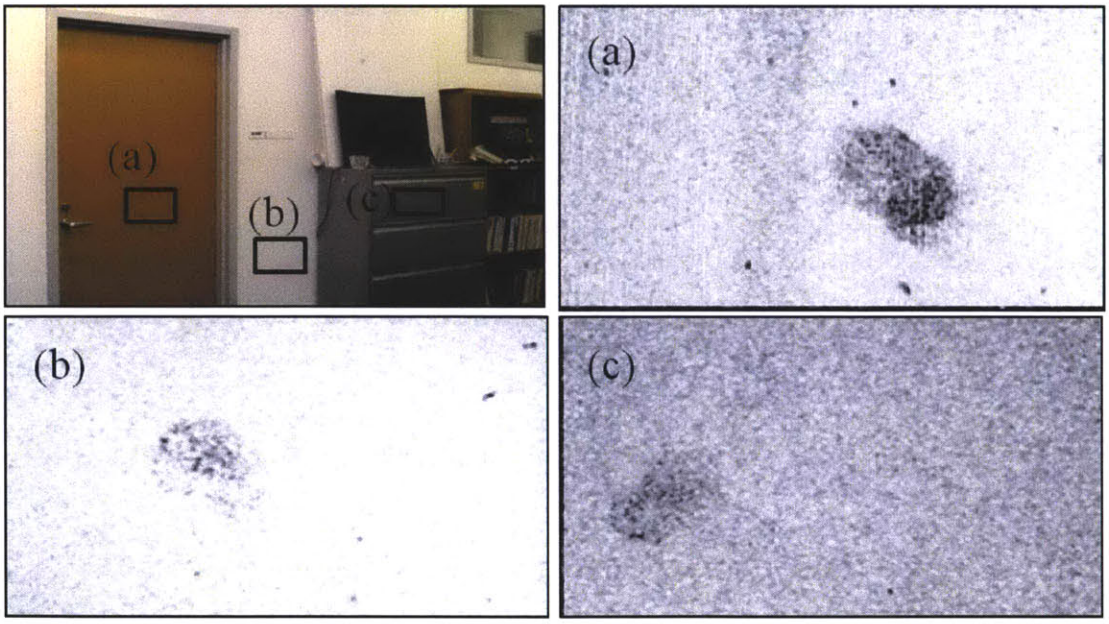

Figure 5-5: Camera viewpoint alignment for flat scenes: (a) door, (b) wall, (c) drawer. For each surface, we first take a reference picture, and then move the system away before gently touching the surface. We then perform the our camera viewpoint alignment scheme on each flat scene to find the viewpoint for the test image. The similarity maps (a)-(c) show that the touched area can be detected by our technique.

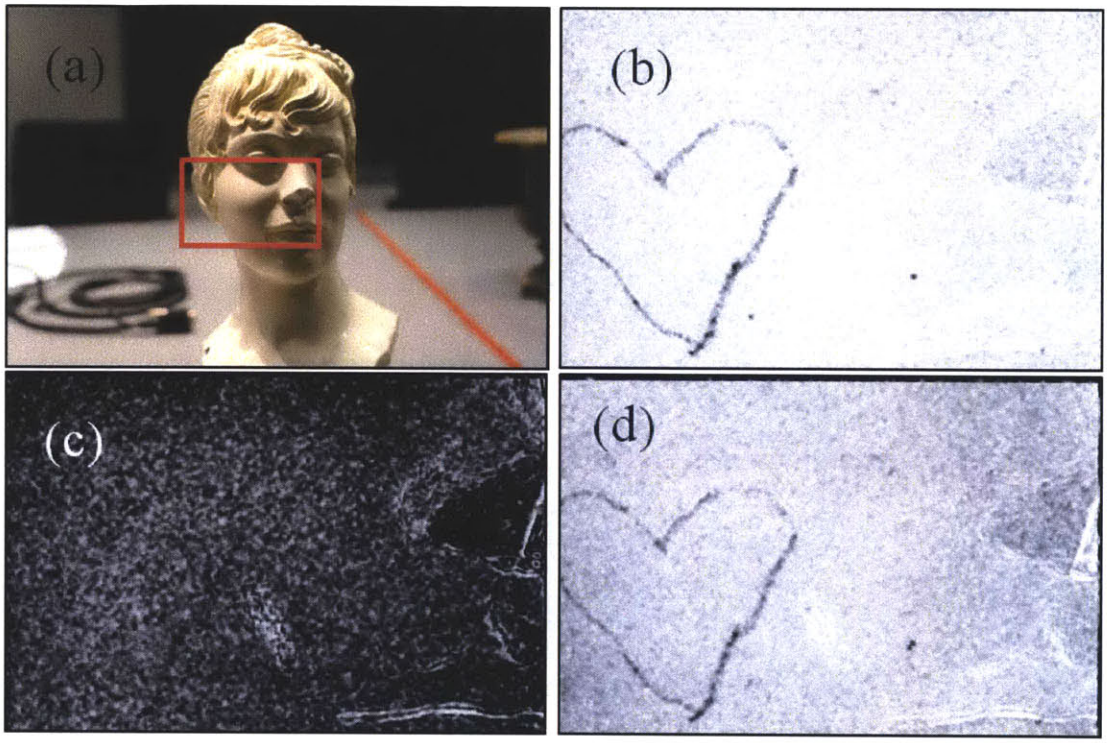

Figure 5-6: Camera viewpoint alignment for a statue of a woman's head (a). We take a reference image, and use a finger to draw a heart on the woman's cheek (in the red rectangle). (b) We calculate the similarity between the reference image and the test images taken without moving the camera, (c) after moving the camera away and using only vision-based rephotography for viewpoint alignment, and (d) using the whole proposed viewpoint alignment method.

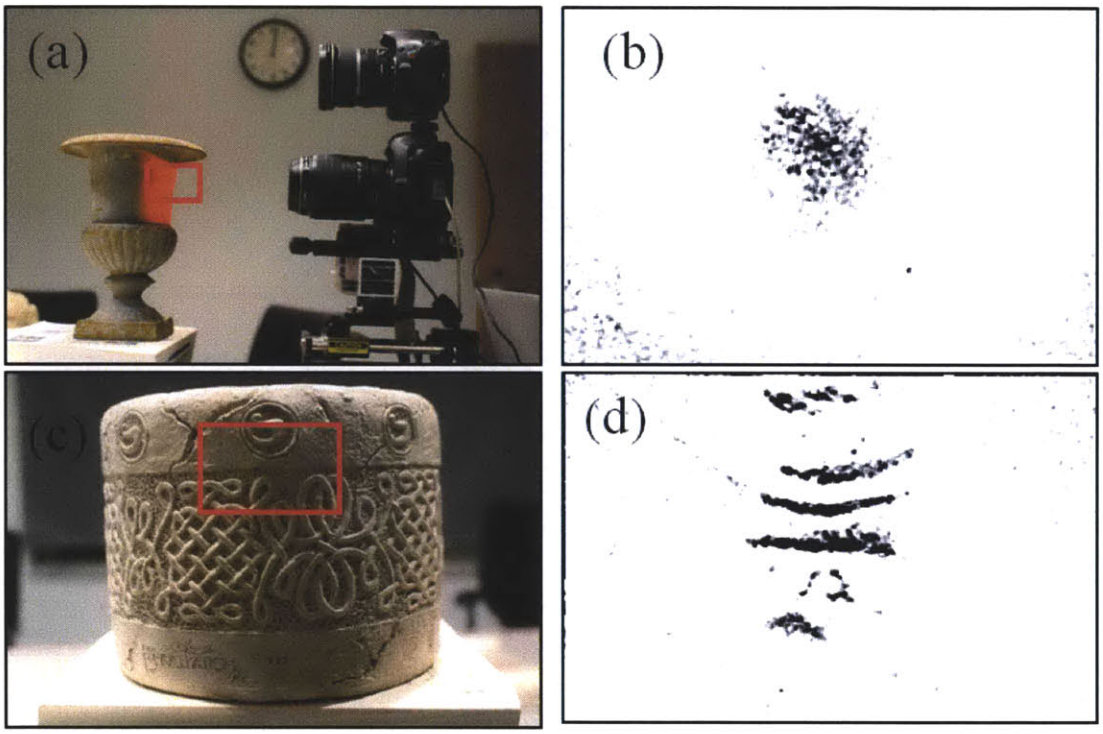

Figure 5-7: Camera viewpoint alignment for two non-planar scenes: (a) a cup (c) a highly textured cylinder. We gently touch the surfaces inside the red rectangle and remove our system from the scene before capturing test images. (b) and (d) show the similarity maps for (a) and (c). Our technique successfully detects the touched regions.

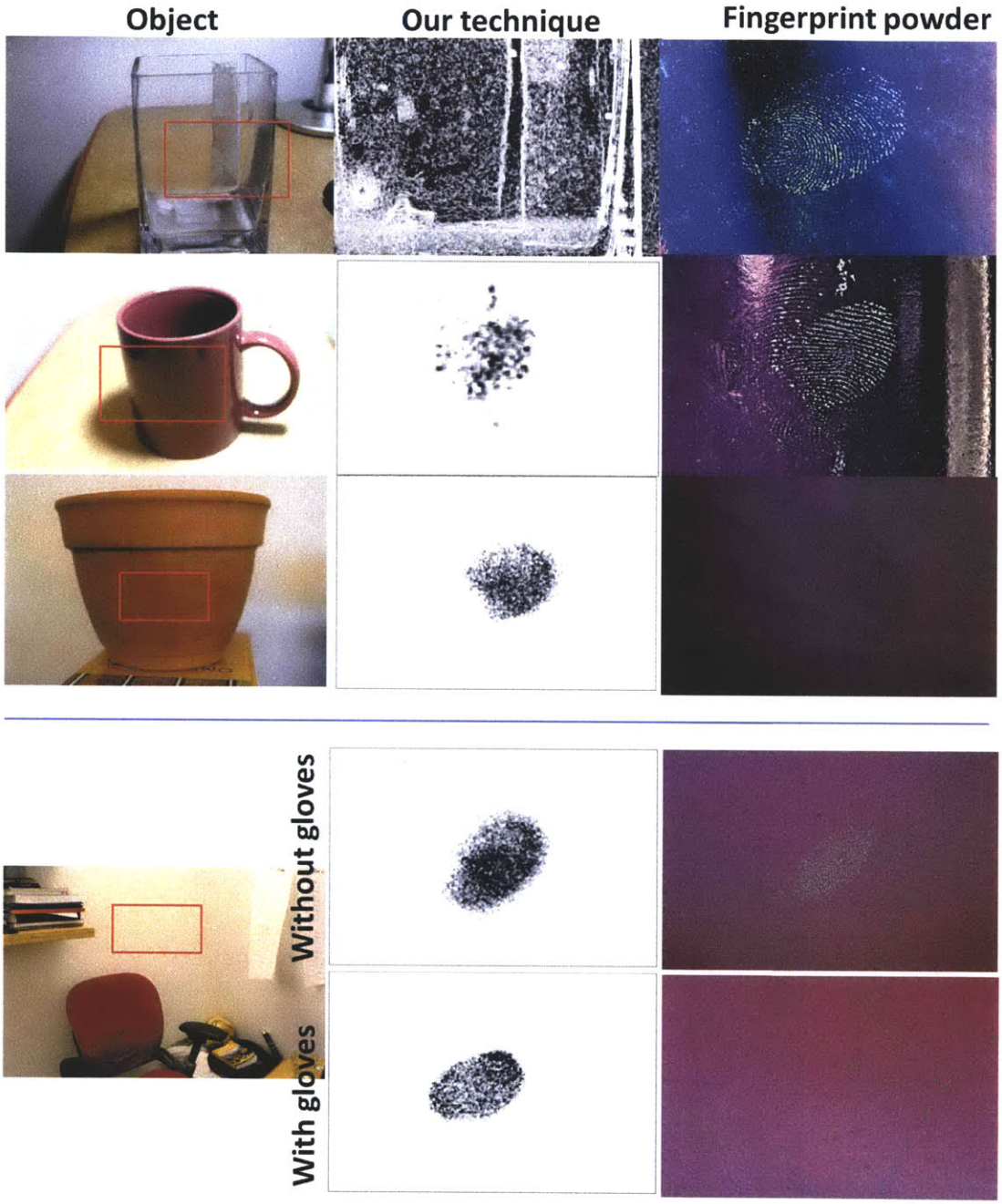

Figure 5-8: We compare our technique to a forensic fingerprinting technique that uses fluorescent powder. We touch different objects using a finger, and show the tampering detection by our technique at the middle column. Then we brush fingerprint powder on the object to detect the latent fingerprint. Our method struggles with transparent objects, while fingerprint powder often fails on porous surfaces. Bottom 2 rows: In the top row we use a bare finger to touch the surface, while in the bottom row we touch the surface with a gloved finger. Fingerprint powder does not work in the latter case, while our technique works in both cases.

Chapter 6

Conclusion

In this work, we presented a technique that can non-invasively detect otherwise-invisible surface tampering by comparing laser speckle images.

Using a combination of vision-based rephotography, structured light, and speckle correlation analysis, we can guide the user within the required viewpoint accuracy of 0.5 mm, typically within five minutes. Our method allows for small surface changes to be detected under very general conditions. We show by our results that human touch, rub, and the weight of a quarter can be detected on very general surfaces. These tampering cannot be detected using a pair of images under normal incoherent lighting.

While the proposed hardware and speckle matching algorithm are simple, the required camera registration is time consuming (about 5 minutes). This part can be improved by automatic rephotography in the future.

There are some possible directions following our work. For example, we want to quantify the surface micro-geometry change using a pair of speckle images, and we want to know the minimum surface tampering our method can detect.

We are interested in exploring other applications of laser speckle using our system. For example, by recording speckle variation over time, we could measure very small object motions. This could let us estimate the mode of the motion, or to re-render the motion in an exaggerated way for visualization [28]. More generally, speckle images are a very discriminative surface representation and could provide the dense features required by a number of applications such as video tracking and 3D scanning. We

hope that techniques such as ours will make these applications available outside the laboratory setting.

Appendix A

Model of Speckle Image Formation

As shown in Fig. A-1, speckle image formation can be modeled by five steps: (a) the incident laser is first scattered by the object surface, and then (b) the field propagates to the lens. Next, (c) the field is modulated by the lens, (d) propagates to the camera senor, and then (e) is recorded by the camera sensor as a speckle image. The propagation steps, (a) and (d), are basically the same operation with different parameters. Here we consider the 1D case. The extension to 2D can be derived by following the same reasoning. The notation and coordinate systems are shown in Fig. A-1.

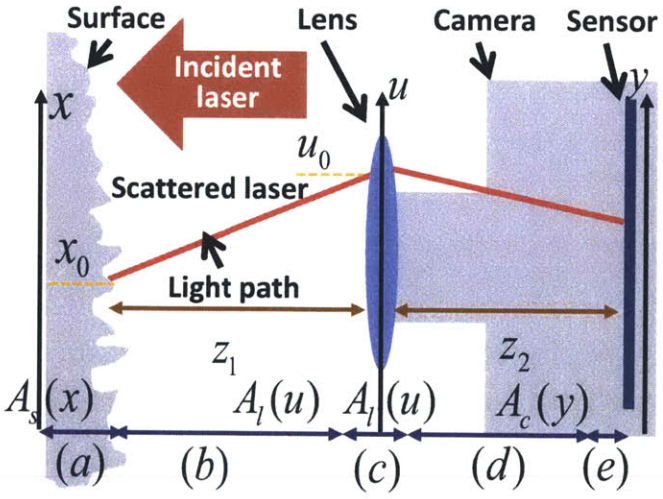

Figure A-1: Left: Speckle image formation can be decomposed as 5 main steps: (a) scattering, (b) propagation between surface and camera lens, (c) lens modulation, (d) propagation between lens and sensor, and (e) image formation at sensor.

Scattering The incident laser field, denoted as $A_{in}(x)$, is modulated by a surface modulation function $e^{jkh(x)}$, where $h(x)$ is the surface height at x, and $k = \frac{2\pi}{\lambda}$ is the wave number for a laser with wavelength λ. The physical meaning of factor $kh(x)$ is the phase change caused by surface height. The scattered field, denoted as $A_s(x)$, is

$$A_s(x) = A_{in}(x)e^{jkh(x)} \ . \tag{A.1}$$

Propagation The field at the lens plane, denoted as $A_l(u)$, receives contributions from every point on the surface,

$$A_l(u) = \int_S A_{x\to u}(x,u)dx \ , \tag{A.2}$$

where S is the surface and $A_{x_0\to u_0}$ represents the field propagated from x_0 on the surface to u_0 on the lens. Each surface point can be regarded as a point light source, whose propagation results in a phase change and attenuation,

$$A_{x_0\to u_0} = A_s(x_0)\frac{e^{jkd_{x_0,u_0}}}{d_{x_0,u_0}} \ , \tag{A.3}$$

where d_{x_0,u_0} is the distance between x_0, u_0. Assuming that the lens-surface distance is large relative to the extent of the imaged area, $z \gg x$, we can write $d_{x,u} \simeq z + \frac{x^2+u^2-2xu}{2z}$ (Fraunhofer far field regime). Together with Eqs. (A.3) and (A.2), this gives us

$$A_l(u) = \frac{e^{j\frac{ku^2}{2z}}}{z}\int_S A_s(x)e^{j\frac{kx^2}{2z}}e^{-jkxu}dx \ , \tag{A.4}$$

ignoring the constant phase term e^{jkz}. This equation shows that the propagation can be decomposed into three basic operations: (1) multiply the attenuated scattered field $A_s(x)$ by a phase factor $e^{j\frac{kx^2}{2z}}$, (2) apply the Fourier transform to the output, and then (3) multiply the output by another phase factor $e^{j\frac{ku^2}{2z}}$ and an attenuation factor $\frac{1}{z}$.

Lens modulation The field modulated by the lens, denoted as $A_{l'}(u)$, is

$$A_{l'}(u) = A_l(u)P(u)e^{j\frac{ku^2}{2f}} \ , \tag{A.5}$$

where $P(u)$ is the aperture function ($P(u) = 1$ if u is on the lens, and $P(u) = 0$ otherwise), and f is the focal length. For the field that passes through the aperture, lens modulation is equivalent to multiplying by a phase factor quadratic in u.

Image formation The relation between the speckle image $I(y)$ and the field propagated to the sensor $A_c(y)$ is

$$I(y) = \|A_c(y)\|^2 \,. \tag{A.6}$$

This describes the fact that the sensor measures the power of the field and does not record phase information. Rather, phase from the surface results in interference patterns in the speckle image.

Speckle equation Combining the above operations, the speckle image can be derived from surface height directly. By assuming that the lens is focused on the surface plane, i.e. $\frac{1}{f} = \frac{1}{z_1} + \frac{1}{z_2}$, and that the incident wave is planar, $A_{in}(x) = A_0$, the speckle image is

$$I(y) = \left\| f\left(-\frac{z_1}{z_2}y\right) \otimes \tilde{g}\left(\frac{y}{z_2\lambda}\right) \right\|^2 \,, \tag{A.7}$$

where $f(t) = \frac{A_0}{z_1} e^{jk\left(h(t) + \frac{t^2}{2z_1}\right)}$ is the input function, $\otimes$ denotes convolution, and $\tilde{g}(\omega) = \mathbb{F}\{P\}$ is the Fourier transform of the aperture function $P(u)$. Figure A-2 shows the simulation using Eq. A.7.

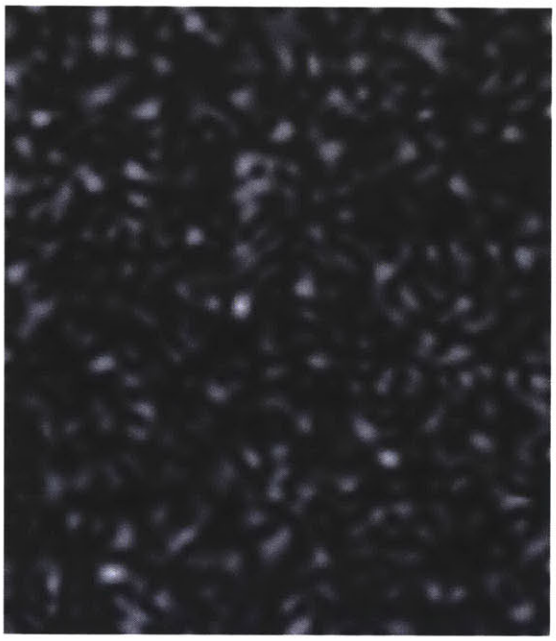

Figure A-2: A speckle image simulated using the 2-D version of speckle image formation equation (Eq. (A.7)), with random surface height and constant incident laser amplitude. The illuminated area is 2 cm by 2 ,cm, and the laser wavelength is 635 nm. The distant between the surface and the camera is 30 cm.

Bibliography

[1] J.D.R. Buchanan, R.P. Cowburn, A.V. Jausovec, D. Petit, P. Seem, G. Xiong, D. Atkinson, K. Fenton, D.A. Allwood, and M.T. Bryan. 'Fingerprinting' documents and packaging. *Nature*, 436(28):475, 2005.

[2] J.W. Goodman. *Speckle phenomena in optics: theory and applications.* Roberts & Co, 2007.

[3] H.J. Rabal and R.A. Braga. *Dynamic laser speckle and applications.* CRC, 2008.

[4] AF Fercher and JD Briers. Flow visualization by means of single-exposure speckle photography. *Optics communications*, 37(5):326–330, 1981.

[5] J.D. Briers and S. Webster. Laser speckle contrast analysis (LASCA): a non-scanning, full-field technique for monitoring capillary blood flow. *Journal of Biomedical Optics*, 1:174–179, 1996.

[6] R.S. Sirohi. *Speckle metrology.* CRC Press, 1993.

[7] J. Zizka, A. Olwal, and R. Raskar. Specklesense: fast, precise, low-cost and compact motion sensing using laser speckle. In *Proceedings of the 24th annual ACM symposium on User interface software and technology*, pages 489–498. ACM, 2011.

[8] S. Bae, A. Agarwala, and F. Durand. Computational re-photography. *ACM Transactions on Graphics*, 29:24:1–24:15, 2010.

[9] R. Pappu, B. Recht, J. Taylor, and N. Gershenfeld. Physical one-way functions. *Science*, 297(5589):2026, 2002.

[10] P.R. Seem, J.D. Buchanan, and R.P. Cowburn. Impact of surface roughness on laser surface authentication signatures under linear and rotational displacements. *Optics letters*, 34(20):3175–3177, 2009.

[11] A. Sharma, L. Subramanian, and E.A. Brewer. Paperspeckle: microscopic fingerprinting of paper. In *Proceedings of the 18th ACM conference on Computer and communications security*, pages 99–110. ACM, 2011.

[12] R. Cowburn. Laser surface authentication-reading nature's own security code. *Contemporary Physics*, 49(5):331–342, 2008.

[13] P.S. Ravikanth. *Physical one-way functions.* PhD thesis, Massachusetts Institute of Technology, 2001.

[14] K. Creath. Phase-shifting speckle interferometry. *Appl. Opt*, 24(18):3053–3058, 1985.

[15] N. Mo and J.C. Shelton. Laser speckle photography to measure surface displacements on cortical bone–verification of an automated analysis system. *Medical engineering & physics*, 20(8):594–601, 1998.

[16] J.R. Fienup. Phase retrieval algorithms: a comparison. *Applied Optics*, 21(15):2758–2769, 1982.

[17] S. Gravel and V. Elser. Divide and concur: A general approach to constraint satisfaction. *Physical Review E*, 78(3):036706, 2008.

[18] H.H. Bauschke, P.L. Combettes, and D.R. Luke. Phase retrieval, error reduction algorithm, and Fienup variants: a view from convex optimization. *JOSA A*, 19(7):1334–1345, 2002.

[19] HML Faulkner and JM Rodenburg. Movable aperture lensless transmission microscopy: a novel phase retrieval algorithm. *Physical review letters*, 93(2):23903, 2004.

[20] J. Goodman. Statistical properties of laser speckle patterns. *Laser speckle and related phenomena*, pages 9–75, 1975.

[21] S.B. Oh, S. Kashyap, R. Garg, S. Chandran, and R. Raskar. Rendering Wave Effects with Augmented Light Field. *Computer Graphics Forum (Proc. EUROGRAPHICS)*, 29(2):507–516, 2010.

[22] Z. Zhang and M. Levoy. Wigner distributions and how they relate to the light field. In *Computational Photography (ICCP), 2009 IEEE International Conference on*, pages 1–10. IEEE, 2009.

[23] A. Adams, D.E. Jacobs, J. Dolson, M. Tico, K. Pulli, E.V. Talvala, B. Ajdin, D. Vaquero, H. Lensch, M. Horowitz, et al. The Frankencamera: An experimental platform for computational photography. *ACM Transactions on Graphics (Proc. SIGGRAPH)*, 29:29:1–29:12, 2010.

[24] Georg Klein and David Murray. Parallel tracking and mapping for small AR workspaces. In *Proc. Sixth IEEE and ACM International Symposium on Mixed and Augmented Reality (ISMAR'07)*, November 2007.

[25] Takashi Okamoto and Toshimitsu Asakura. III: The statistics of dynamic speckles. *Progress in Optics*, 34:183–248, 1995.

[26] H.J. Tiziani. A study of the use of laser speckle to measure small tilts of optically rough surfaces accurately. *Optics Communications*, 5(4):271–276, 1972.

[27] M. Freeman, M. Champion, and S. Madhavan. Scanned Laser Pico-Projectors: Seeing the Big Picture (with a Small Device). *Optics and Photonics News*, 20(5):28–34, 2009.

[28] Ce Liu, Antonio Torralba, William T. Freeman, Frédo Durand, and Edward H. Adelson. Motion magnification. *ACM Transactions on Graphics (Proc. SIGGRAPH)*, 24:519–526, 2005.